Effect of particle-vibration coupling on single-particle states: A consistent study within the Skyrme framework

Gianluca Colò,[1] Hiroyuki Sagawa,[2] and Pier Francesco Bortignon[1]
[1]*Dipartimento di Fisica, Università degli Studi di Milano and Istituto Nazionale di Fisica Nucleare, Sezione di Milano, via Celoria 16, 20133 Milano, Italy*
[2]*Center for Mathematical Sciences, University of Aizu, Aizu-Wakamatsu, Fukushima 965-8560, Japan*
(Received 5 August 2010; published 13 December 2010)

We discuss calculations of the single-particle states in magic nuclei, performed within the particle-vibration coupling (PVC) approach by using consistently the Skyrme effective interaction. The vibrations are calculated within fully self-consistent random-phase approximation and the whole interaction is also used in the PVC vertex. Our main emphasis is therefore the discussion of our results in comparison with those in which some approximation is made. The perspectives for improving current density functional theory (DFT) calculations are also addressed.

DOI: 10.1103/PhysRevC.82.064307 PACS number(s): 21.10.Pc, 21.60.Jz

I. INTRODUCTION

The nuclear implementation of density functional theory (DFT), namely, the mean-field calculations based on effective interactions, are believed to be the most microscopic way to study in a systematic way the ground states and excitations of medium-heavy and heavy nuclei (up to the limiting case of infinite nuclear matter). This is in keeping with the fact that the so-called *ab initio* approaches cannot be used except for light nuclei.

There are different studies carried out by mean-field practitioners. On the one side, several groups are trying to apply existing models to more neutron-rich or proton-rich nuclei, as well as to exotic excited states (e.g., pygmy resonances), to test the performances of the different parameter sets and/or to suggest improvements. At the same time, there are attempts to link the mean-field models to more basic theories such as Brückner-Hartree-Fock or even in-medium QCD. For a general review on mean field models, one can consult Ref. [1].

However, the basic question underlying any kind of mean-field approach concerns the understanding of which many-body correlations are effectively included implicitly (no matter whether one starts from an effective two-body interaction or directly from an effective functional). The DFT purists argue that if a functional is general enough, that is, if it includes the most general density dependence allowed by symmetry considerations, it should, in principle, provide accurate results for variational quantities such as the total energy. One possible objection is whether this is possible in practice: If the density dependence is rather involved and the associated parameters are many, the guideline provided by explicit calculations of the many-body correlations should be quite useful. At the conceptual level, however, the more serious problem is associated with the fact that there are quantities that, strictly speaking, do not belong to the DFT framework, such as the single-particle (s.p.) states.

In this case (as for other observables), two possible routes can be undertaken. Some authors [2–5] are currently trying to improve the accuracy of present DFT implementations aiming at functionals with so-called "spectroscopic" accuracy (referring to, of course, s.p. spectroscopy). In this case, the Kohn-Sham theorem applied to finite nuclei (see Ref. [6] for a recent contribution about open problems on this issue) only guarantees that the energy of the lowest state with given quantum numbers can be exact if the functional is exact. However, within that route, one cannot solve the problem of evaluating the fragmentation of the s.p. strength and, in particular, the so-called spectroscopic factors. Another point of view, which lies at the basis of the present piece of work, is to generalize the shell model to the so-called "dynamical" shell model [7–10].

In this latter case, one considers the Hartree-Fock description of s.p. states as the first step in a more complete many-body description. The s.p. properties of the system are associated with the s.p. Green's function, which is the solution of the Dyson equation including the self-energy Σ. The self-energy is, in general, nonlocal both in space and in time (or momentum- and energy-dependent). The Hartree-Fock potential can be seen as the lowest-order term of the self-energy. To which extent further corrections are relevant depends, in general, on the many-body system under study. In the case of nuclei, owing to the dominance of collective modes in the low-lying part of the spectrum, coupling of the s.p. states with vibrations (in spherical systems) or rotations (in deformed systems) is believed to provide the main contribution to the s.p. self-energy.

If we restrict our discussion to magic nuclei, calculations of the particle-vibration coupling (PVC) have been performed for many decades and have indicated that the coupling effects are relevant. In particular, the effective mass m^* (to which the density of levels is associated) is found to change from $\approx$0.7 m for levels far from the Fermi energy to higher values close to the bare mass m for levels close to the Fermi energy [7].

Most of the calculations of these effects have been performed at the level of second-order perturbation theory. We use the same approach here. At the same time, somewhat surprisingly, most of these calculations are based on purely phenomenological inputs. In Tables 4.3a and 4.3b of Ref. [7], an extensive review of the results obtained in ^{208}Pb by nine groups in the period 1968–1983 can be found. Rather different frameworks had been adopted, none being fully

self-consistent: s.p. potentials range from harmonic oscillator (HO) to Woods-Saxon (WS) or Hartree-Fock (HF) with Skyrme forces; residual interactions at the particle-vibration vertex are either multipole-multipole forces, forces of Landau-Migdal type, Skyrme forces but with velocity-dependent terms dropped, or even G-matrix interactions. Consequently, although there is *qualitative* agreement about several calculations, it is rather hard to assess seriously the *quantitative* impact of all the approximations done and compare in detail with DFT-based calculations.

The issue is quite burning. As discussed in detail in Ref. [11], if one looks, for example, at neutron states in ^{208}Pb, results from DFT and from different implementations of PVC on top of self-consistent mean field (SCMF) differ substantially among themselves and with the experimental findings. The understanding of this discrepancy being, of course, one of the ultimate goals for the whole nuclear structure community, we undertake a preliminary and quite relevant step in the present work.

The relativistic calculations of Ref. [9] are fully self-consistent, because the whole interaction is considered both to build the phonons within the relativistic random-phase approximation (RRPA) framework and to construct the PVC vertex. Also, those calculations go beyond the simple second-order perturbation theory. However, within the framework of nonrelativistic effective interactions there is no fully self-consistent version of PVC. We are not aware of calculations based on the Gogny interaction, and in the case of Skyrme forces the pioneering calculations of Ref. [8] have neglected the velocity-dependent part of the force when coupling particles with vibrations. Consequently, we deem it to be rather timely to study the PVC effects in magic nuclei based on a fully self-consistent RPA calculation of the vibrations and without dropping any term in the coupling vertex. We present calculations of the energy shift owing to PVC for neutron particle and hole states around the core of two benchmark double-magic nuclei, namely, ^{40}Ca and ^{208}Pb.

We present our formalism in Sec. II and selected results in Sec. III: In particular, we focus on the shifts just mentioned, by commenting the differences between complete calculations and approximate calculations. In Sec. IV we draw our conclusions and discuss perspectives for future work. The Appendix is devoted to the details of the calculation of the full PVC vertex.

II. FORMALISM

We discuss in this section the main theoretical ingredients of our calculations. We start by solving the radial HF equations in a radial mesh. The radial step is 0.1 fm and the mesh extends up to 15 fm in the case of ^{40}Ca. The values are 0.15 and 24 fm in the case of ^{208}Pb. After the HF solution is found, we solve the RPA equations in the usual matrix formulation. The continuum is discretized by imposing box boundary conditions at the upper limit of the radial mesh. Consequently, in addition to occupied states denoted by h in what follows, we obtain unoccupied states that are also labeled by a discrete index p (the corresponding energies are ε_h and ε_p). We do not discuss the details of RPA here because we have used it for several earlier publications (see, e.g., Ref. [12]). The interaction used is SLy5 [13]. We treat tensor in a perturbative way; namely, we introduce the tensor terms on top of SLy5 in the same way (and with the same parameters) as has been done in Ref. [14]. These terms are used to correct the s.p. HF states but they are not introduced at higher order; that is, they are not used in RPA nor they are introduced in the PVC vertex. A consistent treatment of tensor, by using the parameter sets introduced in Ref. [15], will be the subject of a forthcoming work. Tensor within RPA has been introduced recently, in the study of both non-charge-exchange [16] and charge-exchange [17,18] excitations.

In calculating the different multipole responses we have deemed it necessary to check both the sum rules and the properties of specific states that are known to couple strongly to nucleons, that is, the low-lying states. In ^{40}Ca (^{208}Pb) we have calculated natural parity phonons with multipolarity L from 0 to 4 (from 0 to 5). In the RPA model space all the occupied states are included, together with the lowest six unoccupied states having increasing values of the radial quantum number n (for each of the values of l and j that are allowed by selection rules). With this choice, in ^{40}Ca the energy-weighted sum rules satisfy the double commutator value by about 97%. The same is true in ^{208}Pb (only for the 5^- the exhaustion is 95%).

After calculating the RPA phonons, only those having energy smaller than 30 MeV and fraction of the total isoscalar or isovector strength larger than 5% have been considered for the coupling with s.p. states. In the next section, we see that the low-lying 3^-_1 state in ^{40}Ca and the 2^+_1 and 3^-_1 states in ^{208}Pb are the most effective. Their properties are shown in Table I. It is clear that, although their energies are somewhat overestimated with respect to the experimental values as a consequence of the value of m^* associated with the force SLy5 ($m^*/m = 0.70$), the description of the transition probabilities is quite reasonable. The choice of the phonon model space is the only free parameter of the present approach. The phonons we consider are labeled by nL in the following (their energies will be written as ω_{nL}). Introducing noncollective states (and consequently also states far above the giant resonance region and/or higher multipoles) would make it necessary to take seriously into account the issue of the Pauli principle correction and would be outside the spirit of the PVC.

Once we dispose of a model space built with single-nucleon states and phonon states, we calculate the energy of the state i

TABLE I. Properties of the low-lying phonons that contribute most to the PVC in ^{40}Ca and ^{208}Pb. The experimental data are from Ref. [22].

Multipole	Theory		Experiment	
	Energy [MeV]	$B(EL, 0 \to L)$ [e^2 fm^{2L}]	Energy [MeV]	$B(EL, 0 \to L)$ [e^2 fm^{2L}]
^{40}Ca				
3^-_1	3.99	1.14×10^4	3.74	1.80×10^4
^{208}Pb				
2^+_1	5.12	3.02×10^3	4.09	3.10×10^3
3^-_1	4.11	5.96×10^5	2.61	6.21×10^5

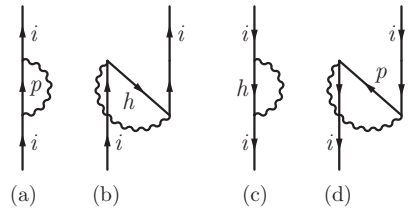

FIG. 1. The four diagrams associated with the single-nucleon self-energy. See the text for details.

by means of second-order perturbation theory, that is,

$$\varepsilon_i = \varepsilon_i^{(0)} + \Delta\varepsilon_i. \tag{1}$$

In this expression, $\varepsilon_i^{(0)}$ is the HF (unperturbed) energy, $\Delta\varepsilon_i$ is the energy shift calculated as $\Sigma_i(\omega = \varepsilon_i^{(0)})$, where Σ_i is the self-energy, and finally ε_i is the corrected (dressed) s.p. energy. The expression of the full second-order self-energy Σ_i is the same as in all previous publications on the subject [7,8]. We report it here for the sake of completeness. It reads

$$\Sigma_i(\omega) = \frac{1}{2j_i+1}\left(\sum_{nL,\ p>F}\frac{|\langle i||V||p,nL\rangle|^2}{\omega-\varepsilon_p-\omega_{nL}+i\eta} + \sum_{nL,\ h<F}\frac{|\langle i||V||h,nL\rangle|^2}{\omega-\varepsilon_h+\omega_{nL}-i\eta}\right), \tag{2}$$

where the s.p. and phonon energies have been defined previously, the (small) imaginary part η is set at 0.05 MeV in the present calculations, and the numerators contain the squared modulus of a reduced matrix element called PVC vertex and discussed below. The two terms on right-hand side of Eq. (2) correspond to the diagrams shown in Fig. 1. In this figure, diagrams (a) and (b) [(c) and (d)] define the self-energy of a particle (hole) state i. Diagrams (a) and (d) correspond to the first term of Eq. (2), whereas diagrams (b) and (c) correspond to the second term of Eq. (2). All four diagrams can be evaluated by standard rules, namely, by associating a matrix element to every vertex and writing appropriate energy denominators: The sum in the first term is over the particle states for the diagrams (a) and (d), while the sum in the second term is over the hole states for the diagrams (b) and (c). The prefactor $1/(2j_i+1)$ in Eq. (2) arises from sum over final states and average over initial states. We now provide details on the calculation of the PVC vertex.

In the case of the coupling with density modes, the basic vertex depicted in Fig. 2 can be calculated starting from the representation of the nth phonon with multipolarity L (here L is the same as the total angular momentum J and parity is the natural one) as

$$|nLM\rangle = \Gamma_n^\dagger(LM)|\mathrm{RPA}\rangle, \tag{3}$$

$$\Gamma_n^\dagger(LM) = \sum_{\mathrm{ph}}\left(X_{\mathrm{ph}}^{nL}A_{\mathrm{ph}}^\dagger(LM) - Y_{\mathrm{ph}}^{nL}A_{\mathrm{ph}}(\widetilde{LM})\right), \tag{4}$$

where A and $A^\dagger$ are standard creation and annihilation particle-hole operators coupled to LM and $|\mathrm{RPA}\rangle$ is the RPA ground-state (cf. also p. 249 of Ref. [19]). If the interaction V is used at the vertex, we obtain for the reduced matrix element

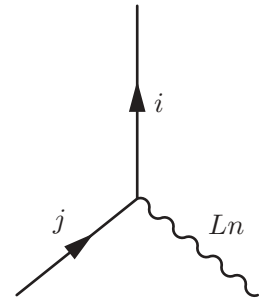

FIG. 2. The basic particle-vibration vertex.

$$\langle i||V||j,nL\rangle = \sqrt{2L+1}\sum_{\mathrm{ph}}X_{\mathrm{ph}}^{nL}V_L(ihjp) + (-)^{L+j_h-j_p}Y_{\mathrm{ph}}^{nL}V_L(ipjh), \tag{5}$$

where V_L is the p-h coupled matrix element,

$$V_L(ihjp) = \sum_{\text{all } m}(-)^{j_j-m_j+j_h-m_h}\langle j_i m_i\, j_j - m_j|LM\rangle \times\langle j_p m_p\, j_h - m_h|LM\rangle \times\langle j_i m_i,\, j_h m_h|V|j_j m_j,\, j_p m_p\rangle. \tag{6}$$

The derivation of formula (5) is provided in the Appendix.

The aim of this work is to consider the full (antisymmetrized) V_{ph}. We include in it the rearrangement terms so that this interaction is the same as that used within the fully self-consistent RPA. So far, the only existing microscopic calculations of the PVC within the Skyrme framework [8] have been performed by using only the (central, velocity-independent) t_0 and t_3 part of the force, that is, by neglecting the velocity-dependent, spin-orbit, and Coulomb terms of V_{ph}. Moreover, the additional approximation used in Ref. [8] was that phonons that are predominantly excited by an external field carrying spin S and isospin T are only coupled through the (S,T) component of the p-h interaction. In our case, we treat properly the spin and isospin degrees of freedom (i.e., without simplifying approximations). We present results which include either the full p-h interaction or the t_0 and t_3 part only. In the latter case, V_{ph} is simply $V_{qq'}(r)\cdot\delta(\vec{r}_1-\vec{r}_2)$ (where the labels indicate that we treat properly the difference between proton-proton, neutron-neutron, and proton-neutron interactions), and the p-h coupled matrix elements reduce to

$$V_L(ihjp) = \frac{i^{-l_i-l_h+l_j+l_p}}{2L+1}\langle i||Y_L||j\rangle\langle p||Y_L||h\rangle \times\int\frac{dr}{r^2}\,V_{qq'}(r)u_i(r)u_j(r)u_p(r)u_h(r), \tag{7}$$

$$V_L(ipjh) = (-)^{L+j_p-j_h}V_L(ihjp),$$

where the radial part of the s.p. wave functions, written as $\phi_{nljm}(\vec{r}) \equiv \frac{u_{nlj}(r)}{r}[Y_l\otimes\chi_{1/2}]_{jm}$, has been introduced. In this simplified case,

$$\langle i||V||j,nL\rangle = \sqrt{2L+1}\sum_{\mathrm{ph}}\left(X_{\mathrm{ph}}^{nL}+Y_{\mathrm{ph}}^{nL}\right)V_L(ihjp). \tag{8}$$

We recall that the radial transition density of the state nL, defined by means of the equation

$$\delta\rho_{nL}^{(q)}(\vec{r}) = \langle nL|\hat{\rho}_q(\vec{r})|\tilde{0}\rangle = \delta\rho_{nL}(r)Y_{LM}^*(\hat{r}), \tag{9}$$

in which $\hat{\rho}_q$ is the density operator and $|\tilde{0}\rangle$ is the RPA ground state, is in fact given by

$$\delta\rho_{nL}^{(q)}(r) = \frac{1}{\sqrt{L+1}}\sum_{\mathrm{ph}\in q}\left(X_{\mathrm{ph}}^{(nL)} + Y_{\mathrm{ph}}^{(nL)}\right)\langle p||Y_L||h\rangle\frac{u_p(r)}{r}\frac{u_h(r)}{r}.$$

As in the discussion before Eq. (7), q is the charge index which labels either neutrons or protons. Then one can also write

$$\begin{aligned}&\langle i||V_{\mathrm{ph}}||j,nL\rangle\\ &= \sum_{\mathrm{ph}}\left(X_{\mathrm{ph}}^{nL} + Y_{\mathrm{ph}}^{nL}\right)\frac{1}{\sqrt{2L+1}}\langle i||Y_L||j\rangle\langle p||Y_L||h\rangle\\ &\quad\times\int\frac{dr}{r^2}\,V_{qq'}(r)u_i(r)u_j(r)u_p(r)u_h(r)\\ &= \langle i||Y_L||j\rangle\sum_{q'}\int dr\;V_{qq'}(r)u_i(r)u_j(r)\delta\rho_{nL}^{(q')}.\end{aligned} \tag{10}$$

In the general case, Eq. (5) cannot be further simplified.

III. RESULTS

Our results for the neutron states of ^{40}Ca are reported in Table II. In the column labeled "SLy5" the bare HF energies $\varepsilon_i^{(0)}$ are displayed. In the next column the same energies are shown when the force "SLy5 + T" of Ref. [14] is employed. In it, the tensor part is added perturbatively on top of SLy5. For ^{40}Ca the tensor effects are almost negligible: This is expected because this nucleus is $\vec{l}\cdot\vec{s}$ saturated and the spin-orbit densities give essentially no contribution to the tensor part of the energy functional and of the mean field (see Ref. [14] for a detailed discussion on this point).

TABLE II. Results for the s.p. neutron energies in ^{40}Ca obtained within HF by employing the Skyrme force SLy5 without (second column) or with (third column) the tensor terms. In the fourth and fifth columns, respectively, the energy shifts and the s.p. corrected energies defined by means of Eq. (1) are provided in the case in which only the velocity-independent part of the Skyrme force (t_0 and t_3 terms) is considered in the PVC vertex. The same values are provided in the next two columns when the full Skyrme force is used in the PVC vertex. Finally, in the last column the experimental energies are shown (from Ref. [23]).

	SLy5	SLy5+T	t_0,t_3 only		Whole Skyrme		
	$\varepsilon^{(0)}$	$\varepsilon^{(0)}$	$\Delta\varepsilon_i$	ε_i	$\Delta\varepsilon_i$	ε_i	$\varepsilon_i^{\mathrm{exp}}$
$1f_{5/2}$	−1.28	−1.26	−3.74	−5.00	−1.55	−2.81	−3.38
$2p_{1/2}$	−3.10	−3.11	−3.44	−6.55	−2.05	−5.16	−4.76
$2p_{3/2}$	−5.29	−5.28	−3.87	−9.15	−2.15	−7.43	−6.76
$1f_{7/2}$	−9.67	−9.69	−2.67	−12.36	−0.95	−10.64	−8.62
$1d_{3/2}$	−15.19	−15.17	−2.25	−17.42	−0.63	−15.80	−15.64
$2s_{1/2}$	−17.27	−17.26	−4.46	−21.72	−1.06	−18.32	−18.19
$1d_{5/2}$	−22.09	−22.10	−0.99	−23.09	−0.29	−22.39	−22.39

In the columns labeled $\Delta\varepsilon_i$ the shifts owing to PVC are displayed. The most evident feature is the strong cancellation between the results obtained with only the t_0 and t_3 (i.e., velocity-independent) part and with the whole Skyrme force at the vertex. An argument to justify this cancellation can be obtained by considering the coupling with a pure isoscalar (IS) phonon (which is appropriate in the case at hand, namely, ^{40}Ca, because isospin is a good quantum number and the low-lying 3^- state is providing most of the effect, as is shown in what follows). The velocity-independent part of the interaction reads

$$V_{\mathrm{ph,\ IS}}^{(t_0,t_3)} = F_0(r)\delta(\vec{r}_1 - \vec{r}_2), \tag{11}$$

where

$$F_0(r) = \frac{3}{4}t_0 + \frac{t_3}{48}\rho^{\alpha}(r)\left[3(\alpha+1)(\alpha+2) + \alpha(1-\alpha)(1+2x_3)\right.$$
$$\left.\times\left(\frac{\rho_n(r)-\rho_p(r)}{\rho(r)}\right)^2\right]. \tag{12}$$

The effect of the velocity-dependent part can be estimated by using the Landau-Migdal approximation (see, e.g., Ref. [20]): within this approximation, one would introduce a correction to the function $F_0(r)$, which is given by

$$\delta F_0(r) = [3t_1 + (5+4x_2)t_2]\frac{k_F^2}{8}. \tag{13}$$

For interior nuclear densities of the order of 0.16 fm^{-3} and associated $k_F = 1.33$ fm^{-1}, the term (13) cancels Eq. (12) by about 75%, while at half density corresponding roughly to the nuclear surface this cancellation is reduced and it is of the order of 50%. It is interesting to notice that these values are qualitatively in agreement with the reduction of the energy shifts, respectively, for holes and particles: The former are in fact expected to be localized more inside the nucleus, with respect to the latter.

To study this point in more detail, we display in Fig. 3 the values of the energy shifts obtained using the Landau-Migdal approximation, in the case of the $f_{7/2}$ neutron state in ^{40}Ca.

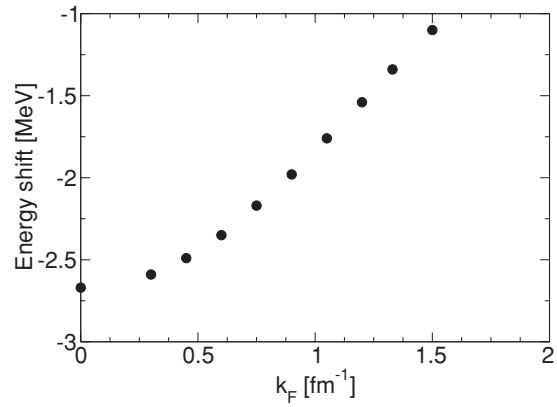

FIG. 3. Shift of the $f_{7/2}$ neutron state in ^{40}Ca, calculated using the Landau-Migdal approximation for the velocity-dependent part of the interaction at the PVC vertex, as a function of adopted values of k_F. It is crucial to remember that the exact value of this energy shift, namely, the one calculated with the full, nonapproximated velocity-dependent interaction, is −0.95 MeV (cf. Table II).

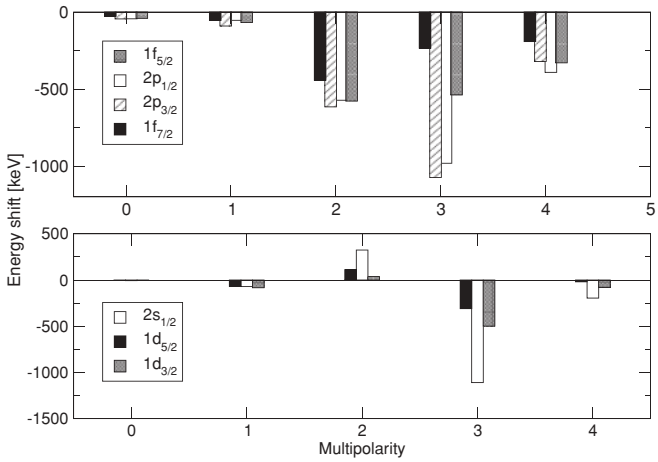

FIG. 4. Separate contributions of the phonons having different multipolarity to the energy shift of the neutron states in ^{40}Ca.

Because the exact value of this energy shift is -0.95 MeV, the Landau-Migdal approximation provides values in reasonable agreement if k_F is taken of the order of 1.33 fm^{-1} or even larger.

Although we have included all phonons according to the prescription of last section, we have clearly identified the low-lying 3^- state as the most effective in producing the energy shifts. In Fig. 4 we display, for all neutron states, the values of $\Delta\varepsilon_i$ obtained from the inclusion in the mass operator of phonons having different multipolarity. It is clear that $L = 3$ is by far dominant owing mainly to the low-lying state, although $L = 2$ plays some role owing to the isoscalar giant quadrupole resonance (ISGQR) and $L = 4$ is also not negligible. The monopole and dipole phonons play a minor role. For particle states, all contributions are negative. This is attributable to the dominance of diagram (a) in Fig. 1: These have negative energy denominators and this does fix their sign, if the state under study is not far from the Fermi energy. Reversing the arguments, one should expect positive contributions for the shifts of the hole states. However, in this case, diagram (c) is associated with hole states having all the same positive parity, and only positive parity phonons, such as the ISGQR, can give non-negligible contributions, because the parity between the hole state (i) and the PV state ($j \otimes L$) in Eq. (2) should be conserved. Thus, only the ISGQR gives a large positive contribution in diagram (c). In the other multipoles with negative parity, such as the 3^-_1 state, diagram (d) in Fig. 1 can contribute to the energy shift. Diagram (d) [first term on the right-hand side of Eq. (2)] has an energy denominator with opposite sign (at least close to the Fermi energy) to the contribution (c) and therefore produces negative shifts as shown in the bottom panel of Fig. 4.

In the last column of Table II the experimental values for the s.p. states (taken from Ref. [23]) are shown so that one can compare with them the energies $\varepsilon_i^{(0)}$ or ε_i. In Fig. 5 the same results are displayed in a way that is more easy to visualize. We have calculated the r.m.s. deviation σ between theoretical and experimental s.p. states. σ is equal to 0.94, 0.95, and 0.62 MeV in the case of SLy5, SLy5 + T, and SLy5 + T plus PVC, respectively. We can conclude that PVC leads to

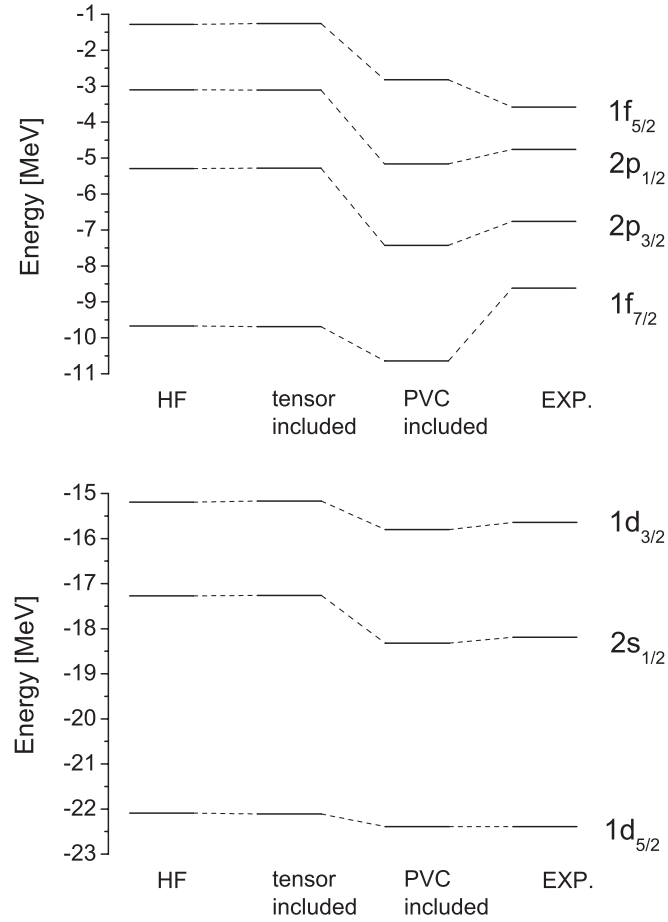

FIG. 5. Neutron states in ^{40}Ca. The four columns, from left to right, correspond to the HF calculation with SLy5 and SLy5 + T, to the HF plus PVC calculation, and to the experimental findings. The values plotted are the same reported in columns 2, 3, 7, and 8 of Table II.

an improvement of the description of these neutron states (although this is not the case if one focuses only on the s.p. gap).

In Table III and Fig. 6, the same results are shown for the case of ^{208}Pb. In this case, the effect of tensor is not negligible (again, as discussed in Ref. [14]). The cancellation in the energy shifts (between the velocity-independent and velocity-dependent part of the vertex function) already found in ^{40}Ca is visible here as well. The energy shifts are, in general, smaller in the present case than in ^{40}Ca. In fact, more occupied states and states with larger angular momenta are involved in the PVC in ^{208}Pb. Owing to this fact, the different contributions (a) and (b) (for particles), or (c) and (d) (for holes), tend to cancel each other, whereas this does not happen in ^{40}Ca.

Also in this case, it is possible to compare either the bare or the dressed s.p. energies with the experimental findings that are shown in the last column of Table III. We have calculated the r.m.s. deviation σ between theory and experiment already discussed for ^{40}Ca. There is still improvement when PVC is included, but it is rather small: In fact, σ is equal to 1.44, 1.51, and 1.21 MeV in the case of SLy5, SLy5 + T, and SLy5 + T plus PVC, respectively. In Ref. [9] it has been found that the PVC on top of the relativistic mean field leads to a

TABLE III. The same as Table II in the case of the neutron states of ^{208}Pb. The experimental s.p. energies shown in the last column are from Ref. [24].

	SLy5	SLy5+T	t_0,t_3 only		Whole Skyrme		
	$\varepsilon^{(0)}$	$\varepsilon^{(0)}$	$\Delta\varepsilon_i$	ε_i	$\Delta\varepsilon_i$	ε_i	$\varepsilon_i^{\rm exp}$
$3d_{3/2}$	0.28	0.34	−0.44	−0.10	−0.32	0.02	−1.40
$2g_{7/2}$	−0.02	0.15	−1.02	−0.87	−0.52	−0.37	−1.45
$4s_{1/2}$	−0.13	−0.10	−0.35	−0.45	−0.23	−0.33	−1.90
$3d_{5/2}$	−0.69	−0.65	−0.67	−1.32	−0.45	−1.10	−2.37
$1j_{15/2}$	−3.65	−1.20	−2.08	−3.28	−0.52	−1.72	−2.51
$1i_{11/2}$	−1.91	−1.02	−0.97	−1.99	−0.32	−1.34	−3.16
$2g_{9/2}$	−3.20	−3.22	−0.71	−3.73	−0.39	−3.61	−3.94
$3p_{1/2}$	−8.15	−8.05	0.05	−8.00	0.04	−8.01	−7.37
$2f_{5/2}$	−9.14	−8.95	0.17	−8.78	0.03	−8.92	−7.94
$3p_{3/2}$	−9.25	−9.19	0.33	−8.86	0.04	−9.15	−8.27
$1i_{13/2}$	−9.41	−10.19	0.27	−9.92	0.08	−10.11	−9.00
$1h_{9/2}$	−12.76	−12.07	0.69	−11.38	0.12	−11.95	−10.78
$2f_{7/2}$	−12.09	−12.07	2.40	−9.67	0.64	−11.43	−9.71

more substantial improvement of this r.m.s. deviation (from 1.92 MeV in the case of NL3 to 0.44 MeV in the case of NL3 plus PVC). The reason for this difference should be further investigated, and we describe in the next section some of the actions that we envisage to undertake.

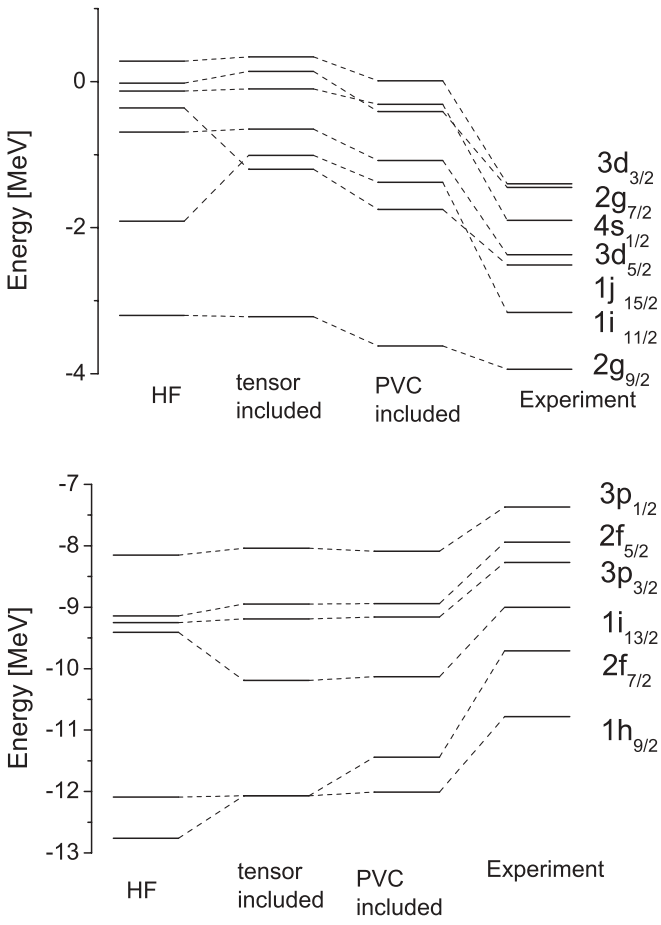

FIG. 6. The same as Fig. 5 for the neutron states in ^{208}Pb.

IV. CONCLUSIONS

Our work is motivated by the fact that, despite many phenomenological calculations and qualitative arguments about the PVC effects in atomic nuclei, only few consistent microscopic calculations are available. In particular, in the case of Skyrme interactions, the only existing calculations are based on approximate evaluations of the PVC vertex in which the velocity-dependent terms are dropped. Therefore, we have implemented a scheme in which the s.p. states are obtained either within HF and or within HF plus PVC, but with the vibrations calculated using fully self-consistent RPA and with the whole Skyrme force employed for the vertices.

In our scheme, second-order perturbation theory is used when PVC is introduced. We have focused on the single-neutron states in both ^{40}Ca and ^{208}Pb and we have analyzed whether bare HF energies, or energies obtained by including the shift owing to PVC, match experiment better. Our main result is that the velocity-dependent part of the Skyrme force tends to reduce the coupling strength to phonons arising from the velocity-independent terms. The resulting shifts are, as a consequence, not very large but rather of the order of ≈MeV in the case of ^{40}Ca and of the order of few hundreds of keV in the case of ^{208}Pb. The dressed single-nucleon energies obtained by summing these shifts to the bare HF energies are in better agreement with experiment than the HF energies. This improvement is more significant in ^{40}Ca than in ^{208}Pb.

The remaining discrepancy with experimental s.p. energies should be further explored. As a future perspective, one should certainly investigate whether perturbation theory is appropriate or not, by comparing with exact solutions of the Dyson equation. Eventually, one expects to be able to judge whether it is possible to match the experimental results by refitting a new Skyrme force and using it in this self-consistent scheme or whether the Skyrme ansatz has problems to be applied at the HF plus PVC level.

APPENDIX: EXPLICIT CALCULATION OF THE PVC VERTEX

We provide in this Appendix the derivation of the reduced matrix element associated with the PVC vertex and written in Eq. (5), namely,

$$v \equiv \langle im_i|V|jm_j, LMn\rangle = \langle 0|a_{im_i} V a^\dagger_{jm_j} \Gamma^\dagger_n(LM)|0\rangle. \quad \text{(A1)}$$

We use definition (4) of the phonon creator operator together with

$$A^\dagger_{\rm ph}(LM) = \sum_{m_p m_h} (-)^{j_h - m_h} \langle j_p m_p j_h - m_h|LM\rangle a^\dagger_{j_p m_p} a_{j_h m_h},$$

$$A_{\rm ph}(\widetilde{LM}) = \sum_{m_p m_h} (-)^{L+M+j_h-m_h} \langle j_p m_p j_h - m_h|L - M\rangle \times a^\dagger_{j_h m_h} a_{j_p m_p}. \quad \text{(A2)}$$

In the case of TDA one could assume that $|0\rangle$ is the HF ground state and apply directly the Wick's theorem. In the case of RPA

phonons, we make the following approximations:

$$v \approx \langle 0|a_{im_i} V \Gamma_n^\dagger(LM) a_{jm_j}^\dagger|0\rangle \approx \langle 0|a_{im_i}[V, \Gamma_n^\dagger(LM)]a_{jm_j}^\dagger|0\rangle. \tag{A3}$$

The commutator appearing in the last expression is

$$[V, \Gamma_n^\dagger(LM)] = \sum_{\rm ph} X_{\rm ph}[V, A_{\rm ph}^\dagger(LM)] - Y_{\rm ph}[V, A_{\rm ph}(\widetilde{LM})], \tag{A4}$$

and we shall call v_1 and v_2 the contributions to v arising from, respectively, the first and the second term in this latter equation. The commutators between V and the operators $A^\dagger$ and A must be evaluated at the same level of approximation as in the RPA, that is, consistently with the linearization of the equations of motion. These commutators can be found, for example, in Ref. [21]. The first one reads

$$\begin{aligned}[V, A_{\rm ph}^\dagger(LM)] &= \sum_{m_p m_h} (-)^{j_h - m_h} \langle j_p m_p j_h - m_h | LM\rangle [V, a_p^\dagger a_h] \\ &= \sum_{m_p m_h} (-)^{j_h + m_h} \langle j_p m_p j_h - m_h | LM\rangle \\ &\quad \times \sum_{\alpha\beta} v_{\alpha hp\beta}\, a_\alpha^\dagger a_\beta,\end{aligned} \tag{A5}$$

and consequently,

$$\begin{aligned}v_1 &= \sum_{\rm ph} X_{\rm ph} \sum_{m_p m_h} (-)^{j_h - m_h} \langle j_p m_p j_h - m_h | LM\rangle \\ &\quad \times \sum_{\alpha\beta} v_{\alpha h\beta p} \langle 0|a_{im_i} a_\alpha^\dagger a_\beta a_{jm_j}^\dagger|0\rangle \\ &= \sum_{\rm ph} X_{\rm ph} \sum_{m_p m_h} (-)^{j_h - m_h} \langle j_p m_p j_h - m_h | LM\rangle v_{ihjp}.\end{aligned} \tag{A6}$$

The second commutator appearing in Eq. (A4) is

$$\begin{aligned}&[V, A_{\rm ph}(\widetilde{LM})] \\ &= \sum_{m_p m_h} (-)^{L+M+j_h - m_h} \langle j_p m_p j_h - m_h | L - M\rangle [V, a_h^\dagger a_p] \\ &= \sum_{m_p m_h} (-)^{L+M+j_h - m_h} \langle j_p m_p j_h - m_h | L - M\rangle \sum_{\alpha\beta} v_{\alpha ph\beta}\, a_\alpha^\dagger a_\beta,\end{aligned} \tag{A7}$$

which gives

$$\begin{aligned}v_2 &= \sum_{\rm ph} Y_{\rm ph} \sum_{m_p m_h} (-)^{L+M+j_h - m_h} \langle j_p m_p j_h - m_h | L - M\rangle \\ &\quad \times \sum_{\alpha\beta} v_{\alpha p\beta h} \langle 0|a_{im_i} a_\alpha^\dagger a_\beta a_{jm_j}^\dagger|0\rangle \\ &= \sum_{\rm ph} Y_{\rm ph} \sum_{m_p m_h} (-)^{L+M+j_h - m_h} \langle j_p m_p j_h - m_h | L - M\rangle v_{ipjh}.\end{aligned} \tag{A8}$$

We are interested in the reduced matrix element defined by

$$\begin{aligned}v &= \frac{1}{\sqrt{2j_i+1}} \langle j_j m_j LM | j_i m_i\rangle \langle i||V||j, nL\rangle \\ &= \frac{(-)^{j_j - m_j}}{\sqrt{2L+1}} \langle j_i m_i j_j - m_j | LM\rangle \langle i||V||j, nL\rangle.\end{aligned} \tag{A9}$$

The contribution to this reduced matrix element which includes the forward RPA amplitudes is, from v_1 in Eq. (A6),

$$\begin{aligned}&\sqrt{2L+1} \sum_{m_i m_j} (-)^{j_j - m_j} \langle j_i m_i j_j - m_j | LM\rangle \sum_{\rm ph} X_{\rm ph} \\ &\quad \times \sum_{m_p m_h} (-)^{j_h - m_h} \langle j_p m_p j_h - m_h | LM\rangle v_{ihjp}\end{aligned} \tag{A10}$$

and this can be written using the p-h coupled matrix elements of Eq. (6) as

$$\sqrt{2L+1} \sum_{\rm ph} X_{\rm ph} V_L(ihjp). \tag{A11}$$

The contribution to the reduced matrix element from v_2 in Eq. (A8) is

$$\begin{aligned}&\sqrt{2L+1} \sum_{m_i m_j} (-)^{j_j - m_j} \langle j_i m_i j_j - m_j | LM\rangle \sum_{\rm ph} Y_{\rm ph} \\ &\quad \times \sum_{m_p m_h} (-)^{L + j_h - m_p} \langle j_h m_h j_p - m_p | LM\rangle v_{ipjh}\end{aligned} \tag{A12}$$

and this can be written as

$$\sqrt{2L+1} \sum_{\rm ph} (-)^{L + j_h - j_p} Y_{\rm ph} V_L(ipjh). \tag{A13}$$

The sum of Eqs. (A11) and (A13) is the result of Eq. (5).

[1] M. Bender, P.-H. Heenen, and P.-G. Reinhard, Rev. Mod. Phys. **75**, 121 (2003).
[2] M. Zalewski, J. Dobaczewski, W. Satula, and T. R. Werner, Phys. Rev. C **77**, 024316 (2008).
[3] M. Kortelainen, J. Dobaczewski, K. Mizuyama, and J. Toivanen, Phys. Rev. C **77**, 064307 (2008).
[4] B. G. Carlsson, J. Dobaczewski, and M. Kortelainen, Phys. Rev. C **78**, 044326 (2008).
[5] B. G. Carlsson *et al.* (unpublished).
[6] B. G. Giraud, J. Phys. G **37**, 064002 (2010).
[7] C. Mahaux, P. F. Bortignon, R. A. Broglia, and C. H. Dasso, Phys. Rep. **120**, 1 (1985).
[8] V. Bernard and N. Van Giai, Nucl. Phys. A **348**, 75 (1980).
[9] E. Litvinova and P. Ring, Phys. Rev. C **73**, 044328 (2006).
[10] G. Colò, H. Sagawa, and P. F. Bortignon, AIP Conf. Proc. **1165**, 267 (2009).
[11] P. F. Bortignon, G. Colò, and H. Sagawa, J. Phys. G **37**, 064013 (2010).
[12] G. Colò, P. F. Bortignon, S. Fracasso, and N. Van Giai, Nucl. Phys. A **788**, 173c (2007).
[13] E. Chabanat, P. Bonche, P. Haensel, J. Meyer, and R. Schaeffer, Nucl. Phys. A **635**, 231 (1998).
[14] G. Colò, H. Sagawa, S. Fracasso, and P. F. Bortignon, Phys. Lett. B **646**, 227 (2007); **668**, 457 (2008).
[15] T. Lesinski, M. Bender, K. Bennaceur, T. Duguet, and J. Meyer, Phys. Rev. C **76**, 014312 (2007).

[16] L. G. Cao, G. Colò, H. Sagawa, P. F. Bortignon, and L. Sciacchitano, Phys. Rev. C **80**, 064304 (2009).
[17] C. L. Bai, H. Sagawa, H. Q. Zhang, X. Z. Zhang, F. R. Xu, G. Colò, and F. R. Xu, Phys. Lett. B **675**, 28 (2009).
[18] C. L. Bai, H. Q. Zhang, X. Z. Zhang, H. Sagawa, and G. Colò, Phys. Rev. C **79**, 041301(R) (2009).
[19] D. J. Rowe, *Nuclear Collective Motion* (Methuen, London, 1970).
[20] N. Van Giai and H. Sagawa, Phys. Lett. B **106**, 379 (1981).
[21] A. M. Lane, *Nuclear Theory* (W. A. Benjamin, New York, Amsterdam, 1964).
[22] [http://www.nndc.bnl.gov].
[23] A. Oros, Ph.D. thesis, University of Köln, 1996.
[24] P. Ring and E. Werner, Nucl. Phys. A **211**, 198 (1973).